Materials Science & Engineering C xxx (xxxx) xxx

Contents lists available at ScienceDirect

Materials Science & Engineering C

journal homepage: www.elsevier.com/locate/msec

# Nanocomposite fibrous scaffold mediated mandible reconstruction and dental rehabilitation: An experimental study in pig model

P.S. Unnikrishnan [a], Subramania Iyer [b], V. Manju [c], C.R. Reshmi [a], Deepthy Menon [a], Shantikumar V. Nair [a], Manitha Nair [a,*]

[a] Centre for Nanosciences and Molecular Medicine, Amrita Vishwa Vidyapeetham, Kochi 682041, India
[b] Centre for Plastic and Reconstructive Surgery, Amrita Institute of Medical Science and Research Centre, Kochi 682041, India
[c] School of Dentistry, Amrita Institute of Medical Science and Research Centre, Kochi 682041, India

ARTICLE INFO

*Keywords:*
Mandibular reconstruction
Dental implant, nanocomposite
Fiber-reinforcement
Osseointegration
Large animal model

ABSTRACT

Mandible reconstruction and dental rehabilitation after trauma or tumor resection represent a serious challenge for maxillofacial surgeons. This study aimed to investigate the bone formation potential of nanocomposite fibrous scaffold (silica-nanohydroxyapatite-gelatin reinforced with poly L-lactic acid yarns - CSF) for delayed Titanium (Ti) implantation, which was compared to autograft (AG) taken from the iliac crest. The grafts were placed in critical-sized mandibular defects in an adult pig model for 6 months followed by dental implant placement for another 3 months. There was complete union and vascularised lamellar bone formation within 6 months. Moreover, the biological processes associated with angiogenesis, bone maturation and remodelling were seen in CSF, which was comparable to AG. Later, when Ti dental implant was placed on newly formed bone, CSF group demonstrated better osseointegration. In short, nanocomposite fibrous scaffold promoted quality bone formation in mandible defect that leads to successful osseointegration, suggesting as a potential candidate for implant-based rehabilitation in clinics in future.

## 1. Introduction

The reconstruction of mandible is a complex procedure and continues to be a challenge in craniomaxillofacial plastic surgery. The situation that leads to compromised alveolar bone includes trauma and resection of benign and malignant lesions [1]. These defects leave the patient with a functional and aesthetic deficit, especially in the impairment of mastication, deglutition, and speech. According to the global cancer statistics, the annual incidence of head and neck cancers worldwide is more than 800,000 and the most affected part is the jaw bone [2,3]. In these patients, the affected bone is resected and reconstructed with an autograft followed by Ti dental implant placement for functional tooth restoration. Dental implants serve as an artificial analogue of the missing teeth that preserves bone height, increases chewing efficiency and enhances the quality of patient's life [4,5].

The use of free vascularised fibula is the gold standard treatment for mandibular reconstruction, as it possesses osteogenic, osteoconductive and osteoinductive properties [5,6]. However, the use of autograft is associated with many limitations, which include donor site morbidity, surgical infection, restricted availability etc. [1]. On the other hand, the efficacy of biomaterials like hydroxyapatite (HA), tricalcium phosphate (β-TCP), Silica-HA was validated in pre-clinical studies as its chemical composition matches to native bone. The implantation of nanoHA block with silica gel at minipig mandible resulted in 7–15% new bone formation after 5 weeks, which depends on the weight percentage of silica in the block [7]. In another study, local tissue reaction around β-TCP block was compared to β-TCP block grafting and periosteal expansion osteogenesis, wherein new bone formation occurred along with bone graft resorption within 8 weeks in both groups [8]. To increase the alveolar ridge height in non-segmental mandibulectomy followed by radiotherapy, a composite (macroporous biphasic calcium phosphate and collagen membrane) together with autologous graft was utilised. Better osseous colonization with ridge augmentation was observed after 16 weeks when compared to the control group without bone marrow [9]. However, none of these studies investigated the ability of newly formed bone to support implants for dental rehabilitation. Recently, Naujokat et al., developed tissue engineered bone after implanting scaffolds (HA, biphasic calcium phosphate, Ti) alongside bone

* Corresponding author.
*E-mail address:* manithanair@aims.amrita.edu (M. Nair).

https://doi.org/10.1016/j.msec.2021.112631
Received 23 August 2021; Received in revised form 9 November 2021; Accepted 20 December 2021
Available online 27 December 2021

morphogenetic protein-2 (BMP-2) and bone marrow in the greater omentum (ectopic site) and evaluated its efficacy to integrate with Ti implants after 8 weeks, but its role in mandible site needs to be validated [5].

An ideal biomaterial for mandibular reconstruction should promote continuous and superior bone formation as successful implant integration depends on the quality and quantity of newly regenerated bone. Previous studies in our lab have shown the efficacy of a biomimetic, biodegradable and mechanically stable nanocomposite fibrous scaffold [silica coated nanoHA-gelatin reinforced with poly(L-lactic acid) (PLLA) yarns] for bone tissue engineering applications. The fibrous yarns were developed by electrospinning technique and embedded within silica-nanoHA-gelatin matrix [10,11]. The nanocomposite was characterized by high compressive and flexural strength, while retaining its interconnected porosity. It enhanced vascularisation and new bone formation in rat femoral defects [10,11]. The material could also promote bone regeneration in critical sized rabbit mandible defect within 3 months, wherein newly formed bone integrates with Ti dental implant [12,13]. However, the bone architecture of rabbit model does not closely resemble human jaw bone, so an equivalent healing cannot be attained. In order to progress towards clinical translation, it is important to validate the performance of nanocomposite in anatomically and physiologically relevant animal models. Studies have shown that the mandible of adult pig mimics human, having similar bone mineral composition, bone regeneration rate and remodelling capacity [14].

The objective of the study was to assess the suitability of nancomposite fibrous scaffold in supporting new bone formation in critical sized mandibular defect in pig. Further, the osseointegration of Ti implants with newly regenerated bone was evaluated. The bone grafts taken from iliac crest was taken as the control. As per our knowledge, this is the first study that focuses on both bone regeneration and osseointegration (9 months study) in clinically relevant animal model *in vivo*.

## 2. Materials and methods

### 2.1. Nanocomposite fibrous scaffold fabrication

Scalable nanocomposite scaffold (4 cm length × 4 cm breadth × 2 cm height) was fabricated as reported earlier [10,11], with some modifications. Continuous fibrous yarns were developed using a novel electrospinning technique, with an open-ended collector [15]. Poly-L-lactic acid (21% *w/v*) (Mw = 100 kDa; Corbion, Netherlands) solution was loaded into a syringe maintained at +10 kV and injected at a flow rate of 3 mL/h. The fluffy deposit formed at the centre of the collector was drawn to form continuous yarns. In parallel, nanoHA was synthesized by wet chemical synthesis route and coated with silica using tetraethyl orthosilicate as precursor [10,11]. Silica coated nanoHA was dispersed in gelatinous matrix (65:35 ratio) and aligned with 5–7 wt% PLLA yarns. The scaffolds were freeze dried at −20 °C to generate porous structure; cross linked using 0.5% glutaraldehyde solution; washed with distilled water and dried again. The morphology, pore size, distribution of yarns and its internal architecture were analyzed by scanning electron microscope (SEM) (JEOL, JSM-6490LA, Tokyo, Japan).

### 2.2. Experimental animals

The methods and procedures adopted for the management, surgery and care of the animals were approved by the CPCSEA (Committee for the Purpose of Control and Supervision of Experiments on Animals) and Institutional Animal Ethics Committee of Amrita Institute of Medical Sciences and Research Centre, Kochi, India (IAEC/2015/1/1). The experiment was designed using skeletally mature pigs [Large White Yorkshire; female; 6–12 months old; and 80–100 kg]. Prior to experiments, animals were quarantined for 10–14 days for acclimatization under standard laboratory environment. All animals were held under a constant 12/12 h light/darkness regimen, where the temperature (20 ± 5 °C) and relative humidity (50 ± 10%) were kept constant. Postoperatively, the pigs were housed individually and monitored. The pigs were fed twice a day and maintained water ad libitum.

The entire study plan was divided into two parts and outlined in Fig. 1. In the first part, bilateral critical size defect created in pig mandible was replaced with materials [(A) Autograft taken from the iliac crest (AG) on left mandible (B) Nanocomposite fibrous scaffold (CSF) on right mandible] and evaluated for bone tissue regeneration after 6 months ($n = 5$). In the second part, Ti dental implants were placed on the newly formed bone (Two implants on each side of mandible, $n = 10$) and assessed for osseointegration after 3 months.

### 2.3. Mandible defect creation and scaffold implantation (part 1)

The surgical procedure was done in pigs after 12 h of fasting (Fig. 2). The animals were pre-anesthetized intramuscularly with xylazine (2 mg/kg), ketamine (10 mg/kg) and midazolam (0.25 mg/kg). To enable endotracheal intubation, thiopentone sodium (10 mg/kg) and meloxicam (0.2 mg/kg) were administered via peripheral venous catheter in the lateral ear vein. General anaesthesia was maintained with isoflurane (2%) in a circular breathing system. After oral prophylaxis, tooth extraction was performed on premolars in bilateral mandible by reflecting the mucoperiosteal flaps, which gave sufficient access to the mandibular bone. At the level of superior border in the mandible bone, a critical sized defect of 6 $cm^3$ volume (3 cm length × 1 cm breadth × 2 cm height) was outlined using a sterile marker [6]. Using a surgical bur under copious sterile saline irrigation, the mandible bone and the periosteum covering the defect site was removed bilaterally. Simultaneously, scaffold (sterilized using ethylene oxide) was cut to the size of intended pig mandibular defect under sterile condition and AG (cancellous bone of predetermined dimension) was harvested from the iliac crest of each animal. The right and left side of the mandibular defect were reconstructed with CSF and AG respectively and sutured with clinical grade sutures (3–0 polyglactin 910 sutures for subcutaneous layer and 2–0 nylon sutures for skin). For postoperative care, the pigs received antibiotic (ceftriaxone 20 mg/kg body weight) and analgesic (meloxicam 0.2 mg/kg and tramadol) intramuscularly and fed with food mixed with water for 3 consecutive days. The animals were observed for 6 months.

### 2.4. Evaluation of bone tissue regeneration

#### 2.4.1. Gross imaging and X-ray imaging

The mandible bones were dissected and fixed in 10% neutral buffered formalin for 1 month. The defect site with surplus of at least 0.5 cm (in all directions) was resected out using a diamond blade and the defect site was photographed with a digital camera (Nikon D7200, Japan). Further, X-ray imaging was done in Carestream dental X-ray machine (CS 9300, United States).

#### 2.4.2. Micro-CT analysis

The mandible specimens fixed in 10% neutral buffered formalin were subjected to an ultra-high resolution micro-CT scanner (MI Labs, Netherlands) at a tube voltage of 55 kV, current of 0.19 mA and exposure time of 66 ms. Primarily, the mandible specimen was positioned in a scanning bed and the defect site was scanned with an ultra-focus magnification throughout 360° for obtaining high-resolution data. The micro-CT scanned data of each mandible specimen was reconstructed three-dimensionally with a spatial resolution of 60 μm (voxels) using the software provided by the manufacturer (MI Labs Reconstruction 9.0). The reconstructed files were further analyzed using multiple software. Image processing software, Dragonfly Pro, Version 3.6 was used to generate volume-rendered three-dimensional images of mandible specimens.

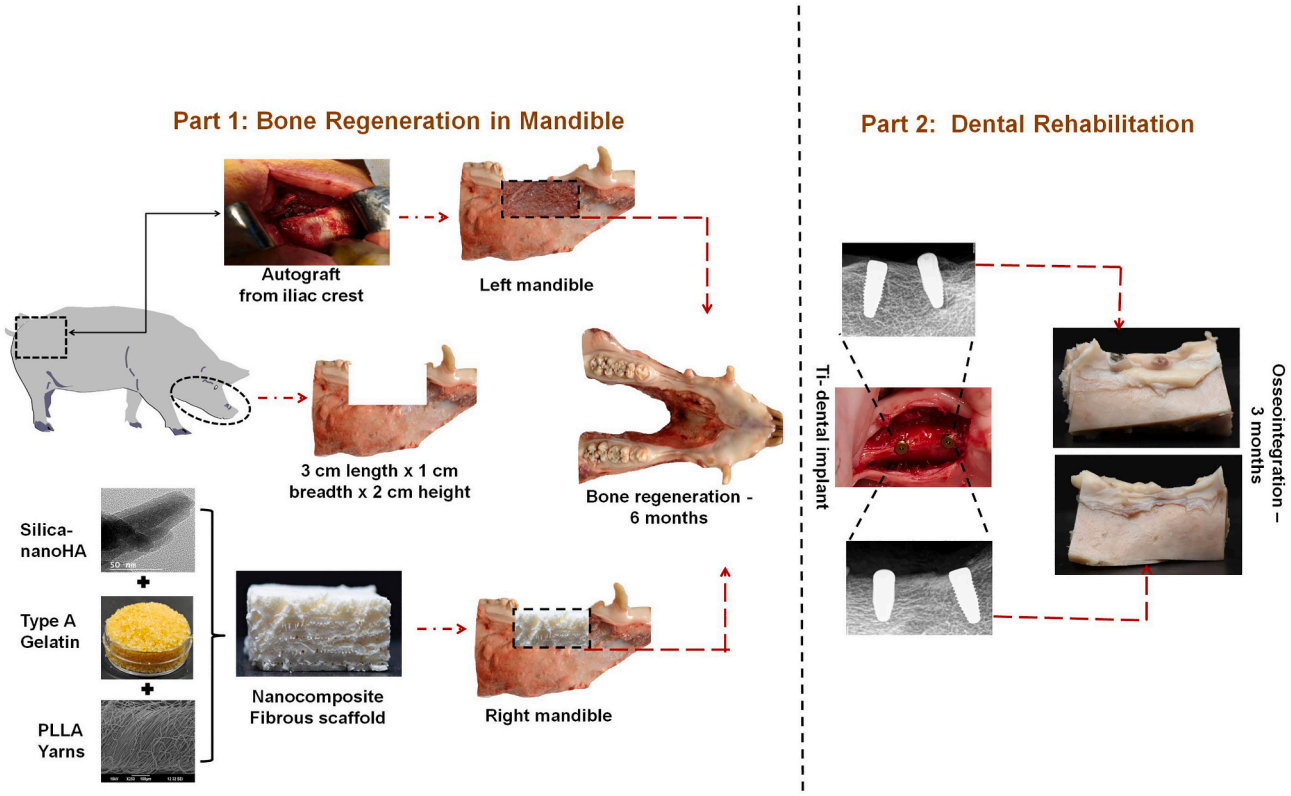


**Fig. 1.** Schematic diagram of the experimental study. Part 1: Bone regeneration study in pig mandible using CSF and AG (representative images shown in right and left mandible are same); Part 2: Ti dental implant placement and osteointegration studies.

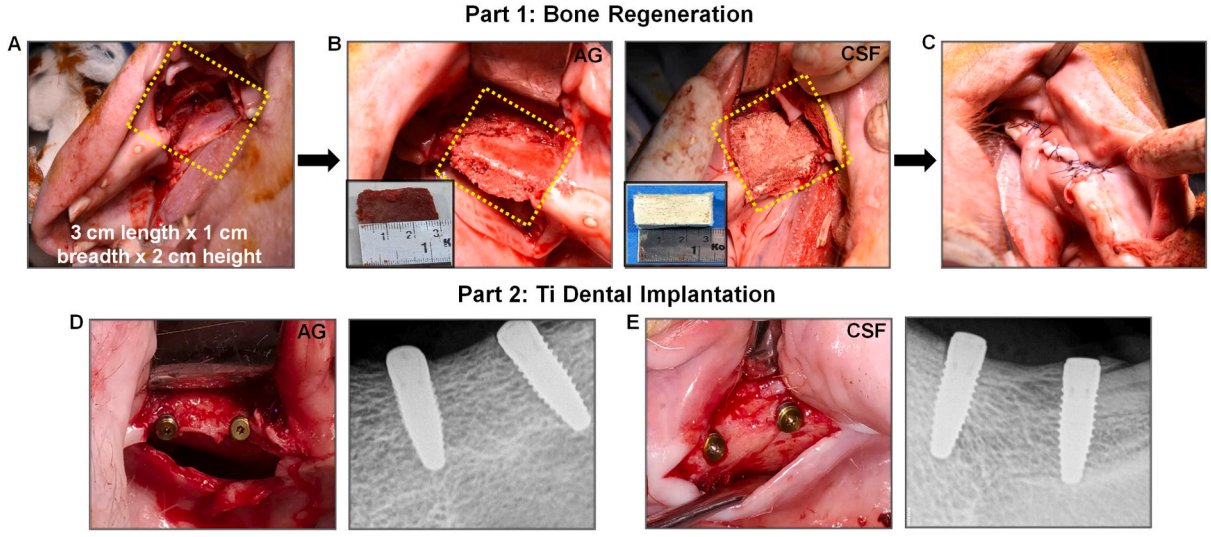


**Fig. 2.** Digital photographs of Surgical implantation and Dental implant integration in Pig mandible (A) Critical sized defect creation (3 cm length × 1 cm breadth × 2 cm height) (B) Materials implantation - AG & CSF (C) Subcutaneous layer suturing (D) Ti dental placement after 6 months of bone regeneration in AG (E) CSF group.

*2.4.3. Histological and histomorphometry analysis*

Following micro-CT scanning, the samples fixed in 10% neutral buffered formalin were cut into two equal halves using a diamond blade. Each half was processed for paraffin and PMMA embedding separately.

*2.4.3.1. Paraffin embedding.* The tissues were decalcified in 12.5% ethylenediaminetetraacetic acid, dehydrated through graded alcohol series (50%, 70%, 80%, 90% and 100%), cleared in xylene, and embedded in paraffin wax. Thin axial sections (5 μm thickness) were taken from the middle region of the tissue using a microtome. The sections were stained with Haematoxylin and Eosin (H&E) as well as Masson's Trichrome to visualize the cellular infiltration and new bone formation. The stained sections were imaged (4× and 10×) with a camera (Nikon DS-Ri1, USA) attached to trinocular light microscope (Nikon Eclipse Ni-E, USA) and further stitched with the help of software.

For quantitative analysis, the defect and host bone area in histology sections were demarcated. The defect area was highlighted by measuring the defect length (2 cm) from top (Mucoperiosteal region) to

bottom of the section and the remaining region was considered as the host bone area. Further, the percentage of new bone area was measured using Fiji-Image J software. The percentage area of new bone formed at the defect site was quantified by marking total bone area of the image as 100%. The percentage of new bone area was calculated as follows.

$$\text{New bone area } (\%) = \frac{\text{Area of bone present at the defect site}}{\text{Total bone area}}$$

The newly formed bone was also evaluated for (a) cortical thickness (b) trabecular thickness and (c) trabecular length. The cortical and trabecular bone was differentiated based on the explanation from previous study [16]. Briefly, the cortical bone refers to the dense bone present at the outer surface of the mandible, whereas the tissue in the individual trabecular structure (mainly inner region) was considered as trabecular bone.

*2.4.3.2. PMMA embedding.* The fixed tissues were dehydrated in increasing concentrations of ethanol (70%, 80%, 90% and 100%) and embedded in polymethylmethacrylate (PMMA). The axial sections (70–100 μm) were taken using linear precision microtome (ACCUTOME100, Struers, Denmark) and polished using a grinder polisher (ECOMET 3000, Buehler, Germany). The sections were stained with Stevenel's blue and Van Gieson's Picro-Fuchsin (Stevenel's blue and van Gieson stains cell nucleus and collagen respectively) and imaged with a trinocular light microscope (Nikon Eclipse Ni-E, USA) under 4× and 10× magnification. Low magnification images (4×) were stitched into a single montage as mentioned in the previous section.

### 2.4.4. Immunohistochemical (IHC) analysis

Decalcified samples were subjected to IHC according to standard protocol. Particular primary antibodies were used to demonstrate vasculature [CD31 - 1:100 (Abcam-ab28364, UK)] and extra cellular matrix deposition [Alkaline phosphatase (ALP) - 1:100 (Abcam-ab224335, UK); Pro-bone morphogenetic protein-2 (BMP2) - 1:100 (Abcam-ab230498, UK) & Osteocalcin (OC) - 1:100 (Abcam-ab13420, UK)] in the newly formed bone. The tissue sections were incubated with primary antibodies overnight at 4 °C and further detected with two step PolyExcel HRP/DAB detection system (PathnSitu, Pleasanton, USA) according to the manufacturer's protocol. The final slides were imaged using a light microscope (Olympus BX51, Japan) at 10 and 20 × magnification.

## 2.5. Ti dental implant placement (part 2)

A critical sized mandible defect was created and reconstructed with CSF and AG using the same surgical procedure mentioned in part 1. After 6 months, the animals were anesthetized, the implant sites (newly formed bone) were drilled sequentially and inserted with four Ti dental implants - 10 mm length × 4.3 mm diameter (Nobel Biocare, Switzerland) in each animal (two at right and two at left mandible) (Fig. S1D-E) ($n = 10$ implants each for both CSF and AG). A distance of 5 mm was maintained between the implants and X-ray was taken to confirm the implant position. Further, flaps were sutured and antibiotics/analgesics were administrated as described above. After 3 months of Ti dental implantation, the animals were euthanized; the mandible containing Ti dental implants was dissected and fixed in 10% neutral buffered formalin.

## 2.6. Evaluation of osseointegration

### 2.6.1. Micro-CT

The formalin-fixed mandible specimens were subjected to an ultra-high resolution micro-CT scanner (MILabs, Netherlands). The images were reconstructed three-dimensionally with a spatial resolution of 20 μm (voxels) using the software provided by the manufacturer (MILabs Reconstruction 9.0) followed by analysis with image processing software (Dragonfly Pro, Version 3.6). Further, the threshold level of Ti dental implants and bone was determined and the percentage of total bone volume (TBV) surrounding the Ti dental implant was calculated with the formula: TBV (%) = Bone volume / Total volume × 100.

### 2.6.2. Histology

The specimens were evaluated for histology by dehydrating with increasing concentrations of ethanol and embedded in PMMA. The sections were stained with Stevenel's blue and van Gieson's picrofuchsin and imaged using trinocular light microscope (Nikon Eclipse Ni-E, USA). The images were first acquired with a 4× magnification, showing the entire implant surface. Large 10× magnification images were also taken for histological evaluation.

### 2.6.3. Histomorphometric analysis

Histomorphometric analysis was performed ($n = 6$) using Fiji-ImageJ software based on previous reports [5], which includes (a) Bone to implant contact (BIC): Measured the bone in contact with implant perimeter starting from the shoulder of the implant (b) Peri-implant bone area (PIBA): Measured the bone area in relation to the total area surrounding the implants up to a lateral distance of 1 mm (c) Inter thread bone area (ITBA): Measured the the area of bone inside the threads in five most central threads on both sides.

## 2.7. Statistical analysis

Results were expressed as mean ± standard deviation and the experimental data was analyzed by Graph-Pad Prism 8. All radiological and histomorphometric data were analyzed using nonparametric Mann-Whitney test. Differences were considered statistically significant if $p$ values were $<0.05$.

# 3. Results

## 3.1. Scaffold characterization

Scalable scaffolds with volume of 32 $cm^3$ were developed for pig implantation study (Fig. 3). Scanning electron micrographs showed that CSF had an open porous structure with average pore size of 150–300 μm. The compressive strength of the biomaterial was about 11.62 ± 4.04 MPa.

## 3.2. Bone regeneration study

### 3.2.1. Clinical observation

Clinical assessment did not reveal any inflammation or infection at the intervention sites. The mucosal membrane and oral cavities were normal. Also, the animals did not exhibit wound dehiscence or scaffold exposure throughout the experiment.

### 3.2.2. Gross and micro-CT imaging

Gross images demonstrated bone and soft tissue healing. Mucoperiosteal flap covering the mandible was intact. The alveolar ridge structure and contour was restored to original form. X-ray and Micro-CT images illustrated bone union and mineralised new bone formation throughout the defect in all the 5 animals in AG and CSF groups. In 3D reconstructive micro-CT images, the progression of structural integration between the new bone and host bone was seen. In both CSF and AG groups, cortical bone was observed at the peripheral region, while trabecular bone in the central region, similar to native mandible. The mean bone volume measured was 8429 ± 2131 $mm^3$ for AG groups and 9083 ± 1294 $mm^3$ for CSF groups. The bone volume / total volume was calculated, which was found to be 19.64 ± 5.5% and 20.89 ± 2.94% in AG and CSF respectively and there were no significant intergroup differences (Fig. 4).

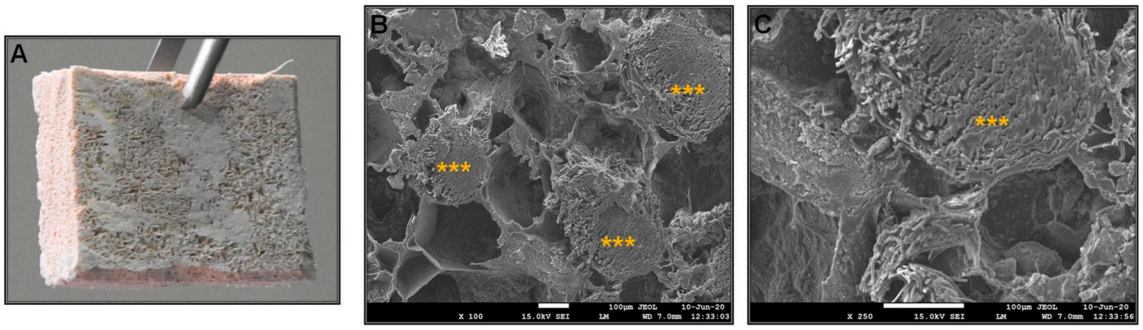


**Fig. 3.** Scaffold characterization (A) Photograph of scalable CSF scaffold (B & C) SEM image of CSF at low (100×) and high (250×) magnification. * indicate yarns.

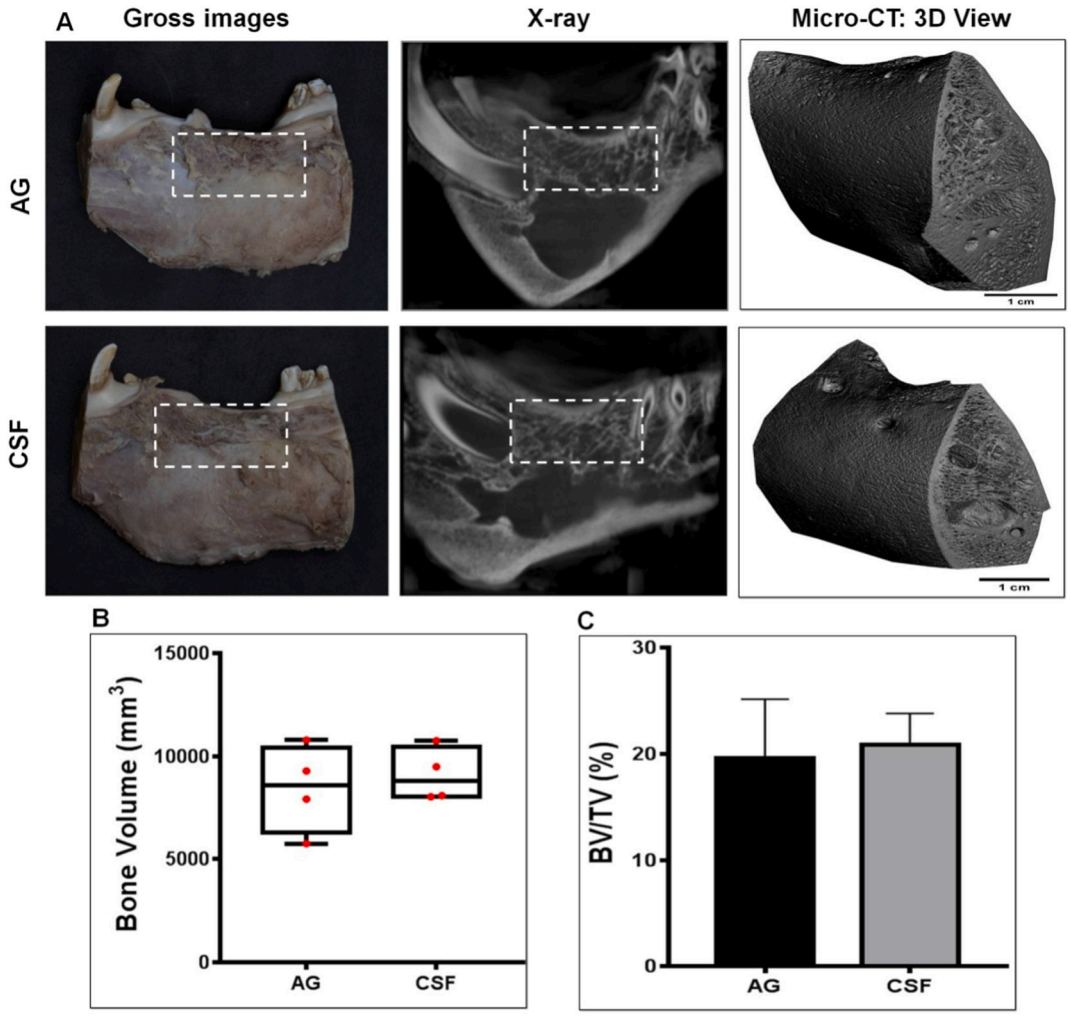


**Fig. 4.** Evaluation of new bone formation (A) Gross, X-ray and Micro-CT images (B) Bone volume and (C) Percentage of Bone volume/Total volume (BV/TV).

*3.2.3. Histological and Histomorphometry analysis*

Histological analysis revealed no signs of degeneration, necrosis, inflammation (macrophages, foreign body giant cells or neutrophils) or fibrous tissue deposition at the defect site. The newly formed bone was covered with mucoperiosteal flap. The connective tissue at flap-bone interface was visible, wherein complete epithelialisation occurred.

H&E staining demonstrated proper integration of new bone into host bone (Fig. 5). As seen in micro-CT, the cortical bone was more prominent at the outer region, while cancellous bone at the inner side (both at the buccal and lingual side) and the spaces between the trabeculae were filled with bone marrow. Higher magnification images demonstrated lamellar bone architecture in both AG and CSF groups. The cortical plates were composed of osteons with Haversian canals and lacunae. Besides, vascular infiltration was seen, both in cortical and cancellous region of AG and CSF groups. Masson's Trichrome Staining confirms the normal bony architecture with collagen fibres (blue dye), osteocytes and blood vessels (Fig. S1). Further, histomorphometric analysis was done, wherein the percentage of new bone around CSF and AG was 88.6 ± 3.04 and 83.35 ± 1.2 respectively. The cortical bone thickness in AG was 1168 ± 120.9 μm, while it was significantly increased in CSF 1597 ± 214.81 μm. However there was no difference in trabecular bone length between AG and CSF groups (Fig. 5A-C).

A portion of bone was also processed for Stevenal's blue and van Gieson's picrofuchsin staining to evaluate the level of material biodegradation. The result showed that there were no material remnants after 6 months. Moreover, a thick cortical bone was clearly evident in those images (Fig. 6).

### 3.2.4. Immunohistochemical analysis

The distributions of bone specific proteins (ALP, BMP-2 and osteocalcin) within the ECM were evaluated in the sections taken from the middle region of newly formed bone (Fig. 7). A mild-moderate immune-positive reaction was observed for ALP and BMP2. Interestingly, the expression of osteocalcin was high (moderate – strong expression), indicating the presence of matured mineralised bone. The endothelial lining of the new blood vessels was confirmed by CD31 staining. Vasculature was detected throughout the newly formed bone in both AG and CSF implanted groups.

### 3.3. Ti dental implantation studies

Titanium dental implants were placed on newly formed bone and its integration was assessed after 3 months (Fig. 8A). Upon exposure of the surgical sites, none of the animals showed loosening of the implant. There was healing in all the animals, without any clinical signs of infection. Mucoperiosteal flap was completely covered and the implant threads were not exposed in any of the CSF implanted groups, but it was slightly visible in two AG implanted groups (2 out of 10 implants). X-ray images confirmed appropriate positioning of the implant in bone. The mineralised bone volume around the implant was analyzed by micro-CT. There was proper implant integration in both CSF and AG groups, but the bone volume was higher in former groups (Fig. 8B).

Further, histology sections were taken and stained with Stevenal's blue and van Gieson's Picrofuchsin (Fig. 9A). At low magnification, the entire implant surface was visible. Most of the implant threads were filled with newly formed bone and bone marrow in CSF and AG groups. When comparing, mineralised bone matrix was seen over the entire implant surface in CSF, while the implants threads in upper region was exposed in AG groups. The percentage of bone-implant contact was statistically higher in CSF (72.85 ± 12.6) than AG (52.53 ± 14.7) (Fig. 9B). Nevertheless, peri-implant bone area and inter thread bone area was similar in both groups (Fig. 9C-D).

## 4. Discussion

The reconstruction of mandible defects due to multiple teeth loss, trauma, or tumor resection is challenging [1]. The treatment includes alveolar bone grafting followed by dental implant placement for aesthetic and functional teeth restoration. Although few biomaterials have shown promising results to support bone regeneration, dental implant integration was not evaluated in those pre-clinical studies. Herein, we have focused on the evaluation of both bone regeneration and dental rehabilitation in pig mandible defect using a biomimetic nanocomposite fibrous scaffold.

Adult pigs were selected as its bone anatomy, healing and remodelling closely mimics humans. The regeneration rate of pigs is similar to humans (pig: 1.2–1.5 mm/day; human: 1.0–1.5 mm/day) [17]. Besides, pig mandible is suitable for mandible reconstruction and dental implant integration studies [18]. However, a pre-requisite for such a model is to understand the critical size defect (defect that will not heal spontaneously) and biomaterial mediated healing time in order to mimic clinical scenario. It is shown that a defect volume larger than 6 $cm^3$ is a critical size defect in pig mandible in the absence of periosteum [6]. Moreover, the reconstruction of large mandible defects in pig model requires six

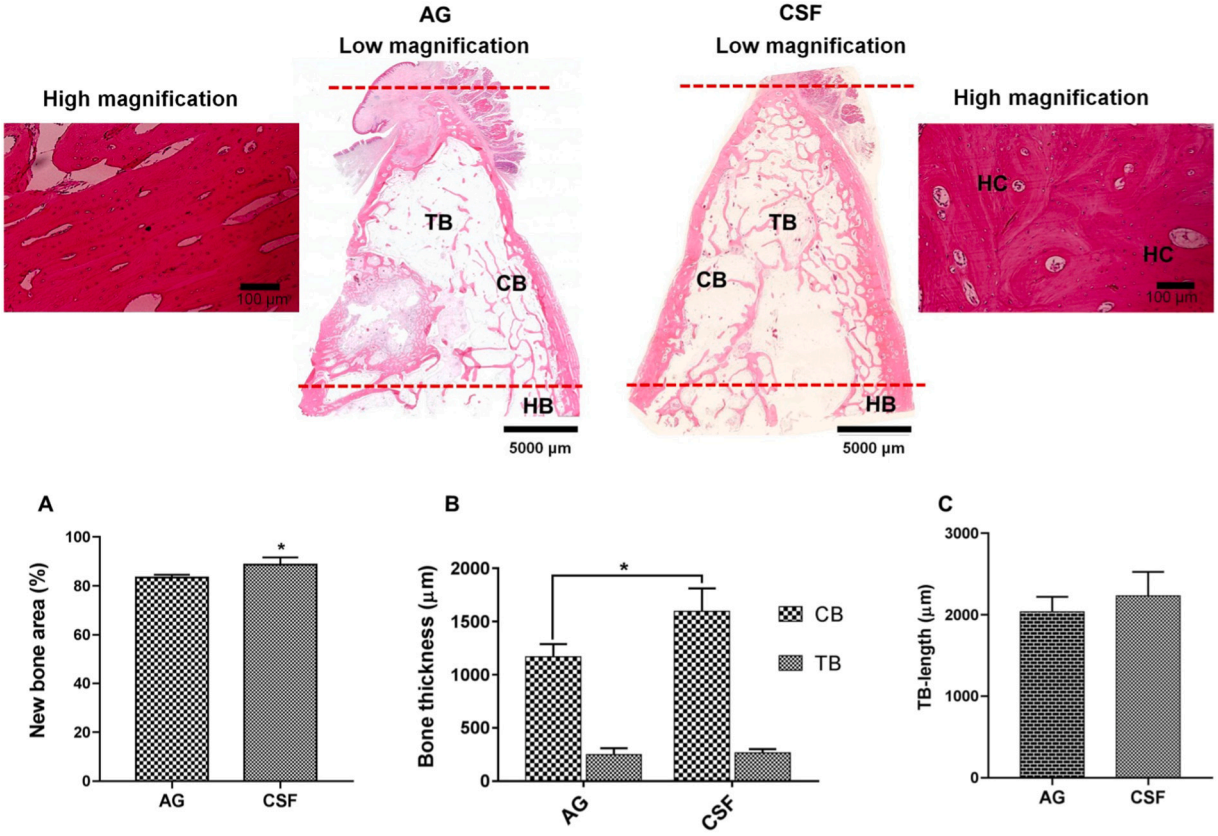


**Fig. 5.** Histological images (H&E staining at low (4×) and high (10×) magnification). Red dotted lines indicate the defect area; CB: Cortical bone; TB: Trabecular bone; HC: Haversian canal. The percentage of new bone and cortical bone thickness was significantly higher in CSF than AG groups ($p$ value: 0.028). (For interpretation of the references to colour in this figure legend, the reader is referred to the web version of this article.)

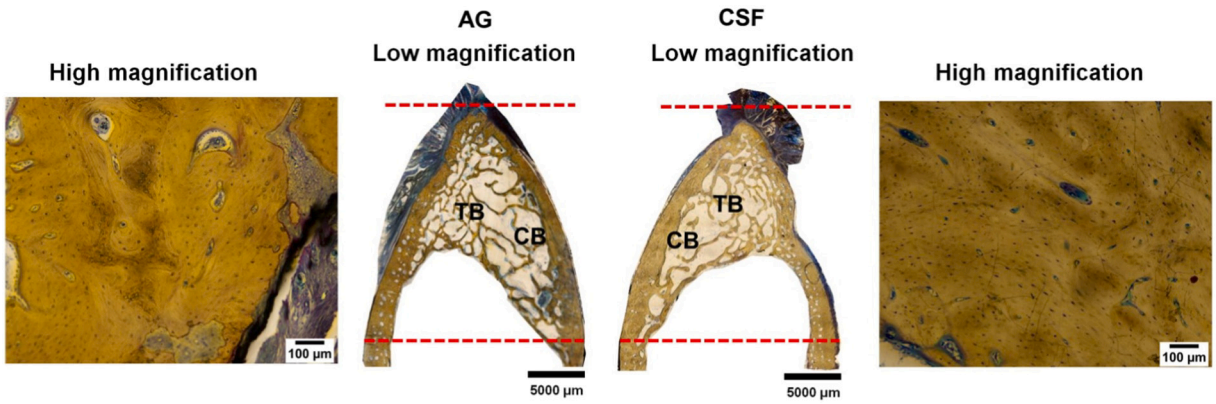


**Fig. 6.** Histological images - Stevenal's Blue and van Gieson's picrofuchsin staining at low (4×) and high (10×) magnification.

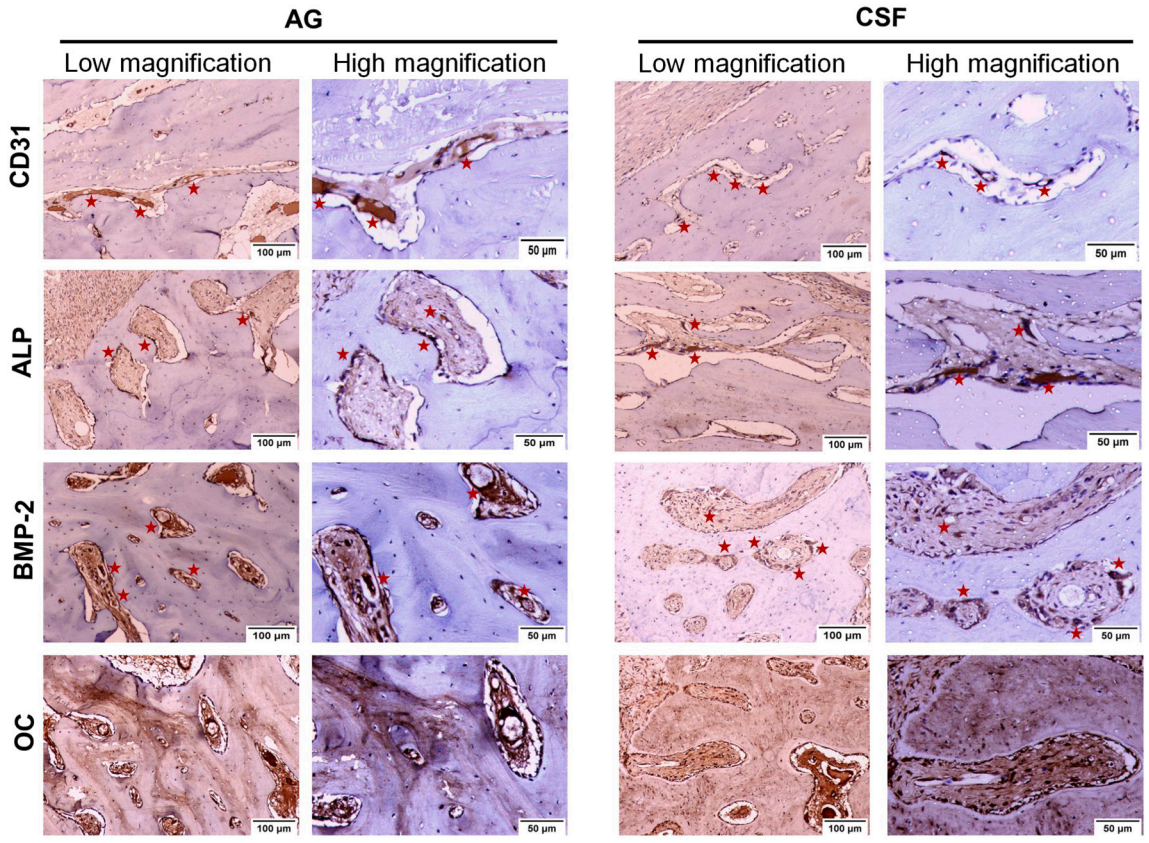


**Fig. 7.** Immunohistochemical analysis of CD31, ALP, BMP-2 and OC. Low (10×) and high (20×) magnification image of AG and CSF implanted groups. Red star indicate the area, which is positive for CD31, ALP and BMP-2. Osteocalcin expression was seen throughout the section. (For interpretation of the references to colour in this figure legend, the reader is referred to the web version of this article.)

months healing time to re-establish its original anatomy [1,19]. Based on those reports, herein, a critical size defect was created (3 cm length × 1 cm breadth × 2 cm height) after removing the periosteum and allowed for 6 months healing.

The successful bone grafting of mandibular defect includes graft transplantation into healthy tissues, recipient area with adequate blood supply, wide contact between adjacent bone and graft and positive fixation [20]. The nanocomposite grafting followed all criteria, except that of mechanical stabilisation, which was avoided to assess its role in providing structural support against masticatory forces and jaw movement. Mastication through crushing and grinding food items invoke a vertical and horizontal force through the tooth root and surrounding alveolar bone [21]. In particular, different stresses including compressive, tensile, shear, and torsional is transferred from the teeth to jaw bones. Herein CSF implanted at mandible region (premolar) was able to withstand the physiological load applied to the jaw bone during mastication. The reinforcement of bioceramic-gelatin matrix with fibrous yarns might have allowed the scaffold to withstand various forces passing through it.

In the first phase, the bone tissue regeneration potential of nanocomposite scaffold was compared to autograft taken from iliac crest. The iliac crest bone was chosen as it is easily accessible and can be contoured to fit segmental mandibular defects [22]. There was bone bridging and union throughout the defect in both CSF and AG groups and the heriarchial organisation (cortical bone at the outer region and cancellous bone with bone marrow in the middle region) was close to native bone.

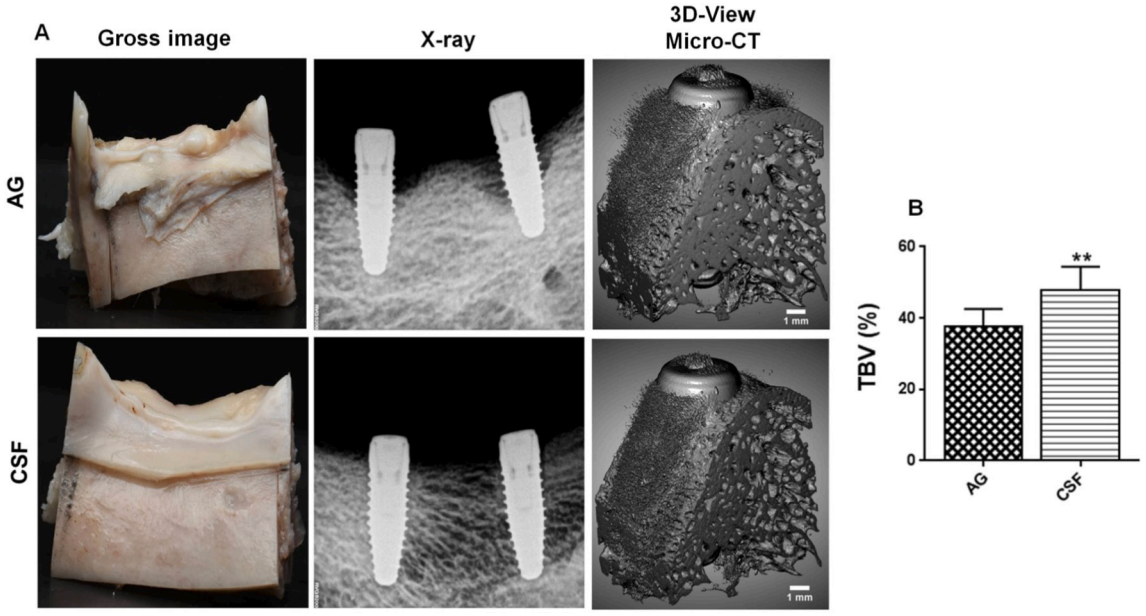


**Fig. 8.** Evaluation of Ti implant integration with new bone (A) Gross image, X-ray and micro-CT (3D-view) (B) Total bone volume (TBV) around the implant. The bone volume in CSF group was significantly higher than AG groups (*$p$ value = 0.007).

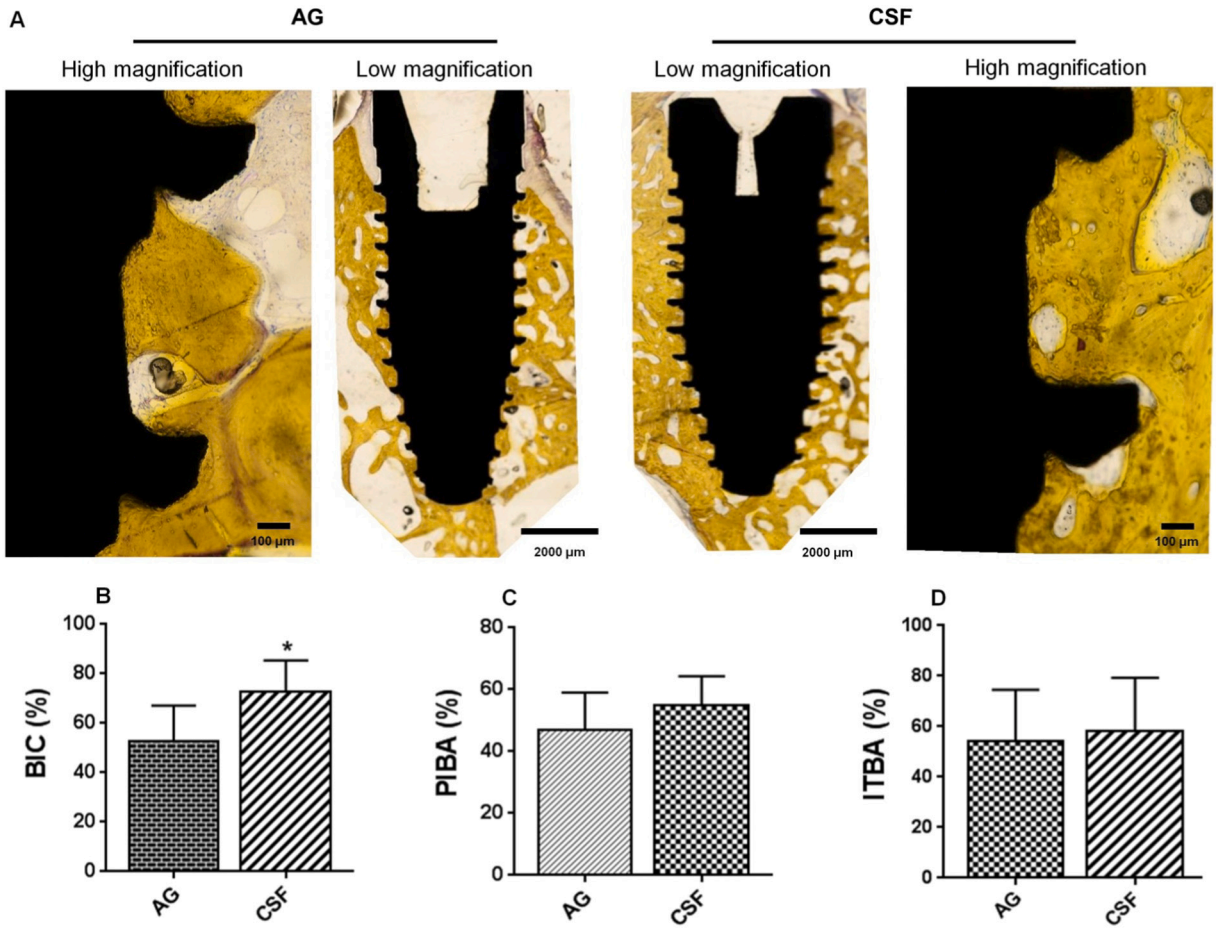


**Fig. 9.** Histology of Ti dental implant integration (A) Histological observation (van Gieson's picrofuchsin staining) at low (4×) and high (10×) magnification showing regenerated bone (golden yellow colour) around Ti dental implant (black) and void spaces (white) (B) BIC (C) PIBA (D) ITBA ($p$ value =0.04). (For interpretation of the references to colour in this figure legend, the reader is referred to the web version of this article.)

This suggests the osteoconductive and osseointegrative nature of nanocomposite fibrous scaffold [19].

The new bone formation is characterized by sequential events involving cell migration, proliferation, osteogenic differentiation followed by mineral deposition and a variety of osteoblast specific markers, including ALP, BMP2, osteopontin, osteocalcin etc., are involved in these processes. Alkaline phosphatase is an early marker and its presence is an indicative of osteoblast activity and osseous deposition, while osteocalcin (the most abundant non-collagenous protein) is expressed during late stages of osteogenesis and mineralization [1,23]. Bone morphogenetic protein-2 regulates osteoblast proliferation and differentiation and is expressed throughout osteogenesis and bone remodelling [24]. In our study, the level of BMP-2 and ALP was mild to moderate, whereas the expression of osteocalcin was strong in both CSF and AG groups. This shows that the process of osteogenesis driven by osteoblast cells was completed and lead to the formation of matured mineralised bone within 6 months [23].

Blood vessel growth and osteoprogenitor infiltration are coupled in bone fractures. Many studies have shown that CD31 positive capillaries represent metabolically active environment in bone tissue with access to oxygen and nutrients. Particularly, a subtype of blood vessels in trabecular and cortical bone (Type H vessels) display high CD31 expression and support osteogenesis [25]. Herein, CD31 expression was analyzed in both CSF and AG groups, which showed a moderate expression. This confirms the neovascularisation in newly formed bone in both the groups. Our previous studies in chicken chorioallantoic membrane and rat femoral models demonstrated that silica containing scaffolds can stimulate vascularisation [10,11]. Silicon ions promote hypoxia inducible factor expression by blocking prolyl hydroxylase domain enzyme and further upregulate angiogenic factors such as vascular endothelial growth factor, basic fibroblast growth factor for angiogenesis [26].

In the second part of the study, the dental implant integration with newly formed bone was studied after 3 months (Commercially available Ti implants were used). The success of an implant depends on its stability, which is determined by the design of implant material, quality of bone surrounding the implant, cortical bone thickness, site of implant placement and loading conditions. In this study, great focus was to evaluate the quality of newly formed bone on dental implant integration. In bones with good regenerative potential (Type III), interfacial milieu is stiffened and, in those areas, when the implants are subjected to loading (whether nominal load or masticatory load), the strain is lowered and support bone formation through Wnt signalling. Nevertheless, in low quality bone, the collagen deposition and mineralization is minimal, resulting in fibrous tissue deposition [27]. Herein, both CSF and AG demonstrated direct apposition of bone with implant without fibrous tissue formation and its BIC was above 60%. This indicates implant stability as clinically successful implants demonstrate 50–80% BIC [28]. Herein silicon ions released from CSF might have enhanced Wnt signalling and Type III bone formation [29]. Moreover, porous gelatin-nanoHA provides an osteoconductive matrix for the infiltration of osteoblast and endothelial cells, resulting in vascularized and functional bone. While there have not been previous studies in engineered scaffolds showing bone healing and osseointegration in critical sized large animal model, direct comparison study cannot be made in this study.

In this study, cortical bone thickness and BIC was better in CSF than autograft. However, it does not demonstrate the superiority of CSF over clinical control AG as the success of an implant is determined not only by biological factors, but also by biomechanical factors. Moreover, the sample number used in the study is less to derive such conclusion. In future, biomechanical properties of newly formed bone shall be studied with a large number of animals in order to understand the translational potential of CSF for mandible reconstruction.

## 5. Conclusion

The present study showed the potential of nanocomposite fibrous scaffold in regenerating new bone in critical sized mandible defects in large animal model. More importantly, the newly formed bone could efficiently integrate with Ti dental implants. In short, the study suggest the usage of nanocomposite scaffold for mandible reconstruction and dental rehabilitation in clinics in future.

Supplementary data to this article can be found online at https://doi.org/10.1016/j.msec.2021.112631.

## CRediT authorship contribution statement

Unnikrishnan P S: Investigation, data curation, writing - original draft.

Subramania Iyer: Study conception/design.

Manju V: Study conception/design.

Reshmi CR and Deepthy Menon: PLLA yarn development and related data analysis.

Shantikumar V. Nair: Study conception/design, Supervision

Manitha B. Nair: Study conception/design, data analysis/interpretation, writing - review & editing and Supervision.

## Declaration of competing interest

The authors declare that there are no conflicts of interest.

## Acknowledgements

The authors acknowledge the funding received from Thematic Projects on Frontiers of Nano Science and Technology (TPF-Nano) Grant, Department of Science and Technology, Government of India. The authors are also thankful to Dr. Rakesh S (Amrita School of Dentistry), Dr. Ajith Nambiar (Department of Pathology, AIMS), and Dr. Sabareeswaran (SCTIMST) for histological analysis. Special thanks to Dr. A.K. K. Unni, Dr. Sreekumar, Dr. Ashok for animal experiments; Dr. Amit G Krishnan for technical help and Dr. Arun Torris, CSIR-National Chemical Laboratory, Pune for Micro-CT analysis.

## References

[1] S. Bhumiratana, J.C. Bernhard, D.M. Alfi, K. Yeager, R.E. Eton, J. Bova, J. M. Gimble, M.J. Lopez, S.B. Eisig, G. Vunjak-Novakovic, Tissue-engineered autologous grafts for facial bone reconstruction, Sci. Transl. Med. 8 (343) (2016), pp. 343ra83-343ra83.

[2] L.Q. Chow, Head and neck cancer, N. Engl. J. Med. 382 (1) (2020) 60–72.

[3] B.R. Manzano, N.G. Santaella, M.A. Oliveira, C.M.F. Rubira, P.S.D.S. Santos, Retrospective study of osteoradionecrosis in the jaws of patients with head and neck cancer, J. Korean Assoc. Oral Maxillofac. Surg. 45 (1) (2019) 21–28.

[4] M. Clementini, A. Morlupi, C. Agrestini, L. Ottria, Success rate of dental implants inserted in autologous bone graft regenerated areas: a systematic review, Oral Implantol. 4 (3–4) (2011) 3–10.

[5] H. Naujokat, Y. Açil, S. Harder, M. Lipp, F. Böhrnsen, J. Wiltfang, Osseointegration of dental implants in ectopic engineered bone in three different scaffold materials, Int. J. Oral Maxillofac. Surg. 49 (1) (2020) 135–142.

[6] F.A. Probst, R. Fliefel, E. Burian, M. Probst, M. Eddicks, M. Cornelsen, C. Riedl, H. Seitz, A. Aszódi, M. Schieker, S. Otto, Bone regeneration of minipig mandibular defect by adipose derived mesenchymal stem cells seeded tri-calcium phosphate-poly (D, L-lactide-co-glycolide) scaffolds, Sci. Rep. 10 (1) (2020) 1–16.

[7] M. Kirchhoff, S. Lenz, K.O. Henkel, B. Frerich, G. Holzhüter, S. Radefeldt, T. Gerber, Lateral augmentation of the mandible in minipigs with a synthetic nanostructured hydroxyapatite block, J. Biomed. Mater. Res. B Appl. Biomater. 96 (2) (2011) 342–350.

[8] K. Yamauchi, T. Takahashi, K. Funaki, Y. Hamada, Y. Yamashita, Histological and histomorphometrical comparative study of β-tricalcium phosphate block grafts and periosteal expansion osteogenesis for alveolar bone augmentation, Int. J. Oral Maxillofac. Surg. 39 (10) (2010) 1000–1006.

[9] F. Jegoux, E. Aguado, R. Cognet, O. Malard, F. Moreau, G. Daculsi, E. Goyenvalle, Alveolar ridge augmentation in irradiated rabbit mandibles, J. Biomed. Mater. Res. A 93 (4) (2010) 1519–1526.

[10] A. Anitha, J. Joseph, D. Menon, S.V. Nair, M.B. Nair, Electrospun yarn reinforced nanoHA composite matrix as a potential bone substitute for enhanced regeneration of segmental defects, Tissue Eng. A 23 (7–8) (2017) 345–358.

[11] A. Anitha, D. Menon, T.B. Sivanarayanan, M. Koyakutty, C.C. Mohan, S.V. Nair, M. B. Nair, Bioinspired composite matrix containing hydroxyapatite-silica core-shell nanorods for bone tissue engineering, ACS Appl. Mater. Interfaces 9 (32) (2017) 26707–26718.
[12] V. Manju, A. Anitha, D. Menon, S. Iyer, S.V. Nair, M.B. Nair, Nanofibrous yarn reinforced HA-gelatin composite scaffolds promote bone formation in critical sized alveolar defects in rabbit model, Biomed. Mater. 13 (6) (2018), 065011.
[13] V. Manju, S. Iyer, D. Menon, S.V. Nair, M.B. Nair, Evaluation of osseointegration of staged or simultaneously placed dental implants with nanocomposite fibrous scaffolds in rabbit mandibular defect, Mater. Sci. Eng. C 104 (2019), 109864.
[14] D. Carmagnola, S. Abati, A. Addis, G. Ferrieri, M. Chiapasco, E. Romeo, G. Vogel, Time sequence of bone healing around two implant systems in minipigs: preliminary histologic results, 2009.
[15] J. John, V.N. Shantikumar, M. Deepthy, Integrating substrateless electrospinning with textile technology for creating biodegradable three-dimensional structures, Nano Lett. 15 (8) (2015) 5420–5426.
[16] S.W. McCormack, U. Witzel, P.J. Watson, M.J. Fagan, F. Gröning, Inclusion of periodontal ligament fibres in mandibular finite element models leads to an increase in alveolar bone strains, PLoS One 12 (11) (2017), e0188707.
[17] M.J. Lopez, Bench to bedside: it's all about the model, Stem Cell Res. Ther. 5 (1) (2014) 1–3.
[18] J. Štembírek, M. Kyllar, I. Putnova, L. Stehlik, M. Buchtova, The pig as an experimental model for clinical craniofacial research, Lab. Anim. 46 (4) (2012) 269–279.
[19] D. Buser, B. Hoffmann, J.P. Bernard, A. Lussi, D. Mettler, R.K. Schenk, Evaluation of filling materials in membrane-protected bone defects. A comparative histomorphometric study in the mandible of miniature pigs, Clin. Oral Implants Res. 9 (3) (1998) 137–150.
[20] B.P. Kumar, V. Venkatesh, K.J. Kumar, B.Y. Yadav, S.R. Mohan, Mandibular reconstruction: overview, J. Maxillofac. Oral Surg. 15 (4) (2016) 425–441.
[21] P.J. Watson, L.C. Fitton, C. Meloro, M.J. Fagan, F. Gröning, Mechanical adaptation of trabecular bone morphology in the mammalian mandible, Sci. Rep. 8 (1) (2018) 1–12.
[22] T.G. Blocker Jr., R.A. Stout, Mandibular reconstruction, World War II, Plast. Reconstr. Surg. 4 (2) (1949) 153–156.
[23] W. Götz, T. Gerber, B. Michel, S. Lossdörfer, K.O. Henkel, F. Heinemann, Immunohistochemical characterization of nanocrystalline hydroxyapatite silica gel (NanoBone®) osteogenesis: a study on biopsies from human jaws, Clin. Oral Implants Res. 19 (10) (2008) 1016–1026.
[24] G.J. Kim, D. Kim, K.J. Lee, D. Kim, K.H. Chung, J.W. Choi, J.H. An, Effect of nano-montmorillonite on osteoblast differentiation, mineral density, and osteoclast differentiation in bone formation, Nanomaterials 10 (2) (2020) 230.
[25] A.P. Kusumbe, S.K. Ramasamy, R.H. Adams, Coupling of angiogenesis and osteogenesis by a specific vessel subtype in bone, Nature 507 (7492) (2014) 323–328.
[26] K. Dashnyam, A. El-Fiqi, J.O. Buitrago, R.A. Perez, J.C. Knowles, H.W. Kim, A mini review focused on the proangiogenic role of silicate ions released from silicon-containing biomaterials, J. Tissue Eng. 8 (2017), 2041731417707339.
[27] F.A. Shah, P. Thomsen, A. Palmquist, Osseointegration and current interpretations of the bone-implant interface, Acta Biomater. 84 (2019) 1–15.
[28] Z. Lian, H. Guan, S. Ivanovski, Y.C. Loo, N.W. Johnson, H. Zhang, Effect of bone to implant contact percentage on bone remodelling surrounding a dental implant, Int. J. Oral Maxillofac. Surg. 39 (7) (2010) 690–698.
[29] P. Han, C. Wu, Y. Xiao, The effect of silicate ions on proliferation, osteogenic differentiation and cell signalling pathways (WNT and SHH) of bone marrow stromal cells, Biomaterials Science 1 (4) (2013) 379–392.